High-Altitude Balloon Test of Satellite Solar Occultation Instrument for Monitoring Stratospheric O_3, H_2O and HNO_3

M. P. WEINREB, W. A. MORGAN, I-LOK CHANG,[1] L. D. JOHNSON, P. A. BRIDGES AND A. C. NEUENDORFFER

NOAA/National Environmental Satellite, Data and Information Service, Washington, DC 20233

(Manuscript received 15 July 1983, in final form 28 November 1983)

ABSTRACT

In June 1982 a multi-detector infrared grating spectrometer was carried by a balloon to an altitude of 39 km at Palestine, Texas, where it measured intensities of solar radiation transmitted by the stratosphere before and during sunset. The instrument detected radiation continuously in eight spectral intervals in the infrared, including two in the 9.6 μm absorption band of ozone, two near 6.6 μm in the water vapor absorption band, and one in the 11.3 μm band of nitric acid. These data permitted retrievals of concentrations of ozone, water vapor and nitric acid at 1 km intervals between the altitudes of 25 and 39 km. The ozone retrieval was compared with *in-situ* measurements made by ECC-sondes, which were available below 32 km. The measurements by the two systems were in good agreement. No *in-situ* data were available to be compared with the retrieved ozone profile above 32 km or with the water vapor and nitric acid retrievals. However, these retrievals agreed qualitatively with other measurements made in past years.

1. Introduction

The possibility that long-term changes are occurring in concentrations of stratospheric trace constituents is currently a topic of concern, because these changes may influence the atmosphere's radiation balance and change the distribution of stratospheric and upper-tropospheric ozone. A monitoring program is the most straightforward way to ascertain whether concentrations of stratospheric constituents are actually changing in the long term. Our interest is in developing a monitoring program conducted with remote-sensing instruments on earth-orbiting satellites. Since satellite-based observations are made over large areas of the globe repeatedly with a single sensor, they are ideal for monitoring.

To be useful for long-term monitoring, a satellite-based sensor must be stable and reliable. It should put out data at a relatively low rate, and it should not be expensive to design and build. These requirements are readily met by an instrument we are considering, a grating spectrometer working in solar occultation, i.e., measuring absorption of solar infrared radiation by the atmosphere's limb. Rather than scanning the infrared spectrum, the spectrometer uses several detectors to sense continuously in a number of discrete spectral intervals located in absorption bands of species of interest. The requirements mentioned above might also be met to some extent by a filter radiometer. In fact, instruments of both types have been used since the late 1960's on satellites of both NOAA and NASA for measuring atmospheric temperatures and constituent concentrations. However, for isolating absorption bands of constituents, the spectrometer is preferred because of its higher resolution and superior spectral purity.

The decision to work with solar occultation rather than atmospheric emission was a consequence of the high intensity of solar infrared radiation. It eliminates the need to cool the instrument with cryogens and to use sophisticated detector technology. It also simplifies the data reduction by eliminating the need for radiative transfer calculations and the attendant need for accurate *a priori* knowledge of the atmospheric temperature profile.

Many aircraft- and balloon-based experiments have been performed to determine concentrations of trace constituents from measurements of solar absorption, with scanning spectrometers (e.g., Murcray *et al.*, 1966), grille spectrometers (Girard *et al.*, 1977), and interferometers (e.g., Farmer *et al.*, 1980; Murcray *et al.*, 1979). These experiments yielded excellent absorption spectra of the atmosphere, which helped us determine the spectral resolution needed to isolate the signals from various species. They also provided information on the characteristics (e.g., accuracies, vertical resolution) of the concentration profiles that can be inferred from the measurements. We concluded

[1] The American University, Washington, D.C. 20016.

© 1984 American Meteorological Society

Unauthenticated | Downloaded 05/19/25 12:36 PM UTC

that a satellite-borne grating spectrometer, as just described, working with moderate spectral resolution (between 0.3 and 5 cm^{-1}), is an appropriate instrument for monitoring the concentrations in the stratosphere of many photochemically important species, including O_3, $CFCl_3$, CF_2Cl_2, CH_4, N_2O, NO_2, CO, H_2O, HNO_3 and perhaps HCl. To demonstrate that this is so, we built a prototype instrument and began a series of balloon flights to test it. The first flight occurred on 21 June 1982 at Palestine, Texas. Observing at sunset from an altitude of 39 km, the instrument collected absorption data on O_3, HNO_3 and H_2O. This paper describes that experiment and its results.

2. Instrumentation

The flight instrument consists of a telescope to collect solar radiation and a spectrometer to disperse and detect it. A layout of the instrument appears in Fig. 1. The telescope is of the Cassegrain type, has a 0.6 m focal length, and brings an $f/4.5$ beam to a focus at the spectrometer's entrance slit. A dichroic filter in front of the entrance slit transmits radiation only with wavelengths greater than 3.5 μm. The shorter wavelength radiation is reflected back into the telescope and illuminates two pairs of detectors. The signals from these detectors keep the instrument pointed at the sun, as described below.

The entrance slit is a rectangle 1.5 mm high and 0.8 mm wide, and it defines a field of view that is 8.3 arc minutes in elevation and 4.5 arc minutes in azimuth. Therefore, the instrument "sees" a fraction of the sun's disc, which subtends 32 arc minutes. The spectrometer has an over/under Ebert layout with a focal length of 0.5 m. Usually in such an instrument the grating rotates to provide spectral scans, but in this instrument the grating is stationary, and there is no scanning. Instead, there are eight separate detectors, which isolate eight discrete spectral intervals in the infrared. Radiation is detected continuously in these intervals and not at all in the rest of the spectrum. This simplifies the data reduction, and it avoids the need for the high data rates that would be required by a scanning spectrometer.

The detectors are evaporated thermopiles. Each has an integral filter-window as an order-sorter. The infrared beam is mechanically chopped at about 4.8 Hz by a symmetrical two-blade chopper behind the entrance slit. The modulated detector output is amplified, synchronously rectified, and filtered with a time constant of $\sim$1.5 s. The resulting signal is digitized and transmitted to earth via 50-kilobit PCM (Pulse-Coded Modulation) telemetry.

The instrument was connected to the gondola by two sets of motor-driven gimbals, which permit rotation in both elevation and azimuth, as is required to keep the instrument pointed at the sun's center. Initial acquisition of the sun is made with a tracking system provided with the gondola by the National Aeronautics and Space Administration, Goddard Space Flight Center. This system works most efficiently at high solar elevation angles. When the sun is near the horizon, a second tracker, consisting of the two pairs of detectors in the telescope, is employed. To minimize the detrimental effects of atmospheric absorption and high background illumination, this tracker was designed to operate in the 2.18 μm atmospheric window and to have a field of view of 0.5°. One pair of the tracker's detectors is located at the upper and lower rims of the sun's image, while the second pair is located on either side of the sun's image. In operation, the difference signals from the two pairs of detectors actuate the gimbal motors. When the sun's image is centered between the two detectors of a pair, both detectors are illuminated equally, and a null difference signal results. However, should the sun's image be offset, the unequal illumination would produce a non-zero difference signal, actuating the associated motor to rotate the instrument and drive the sun's image towards the "centered" condition. In pre-flight tests on the ground, the instrument was able to track the sun with biases and random departures from the centered condition not exceeding 3 arc minutes.

Table 1 lists the eight spectral intervals and the gases being sensed. We decided upon these intervals by inspecting measurements (Goldman *et al.*, 1982) and line-by-line calculations (Neuendorffer, 1977) of high-resolution absorption spectra through stratospheric limb paths. We sought intervals with a reasonable percentage of absorption (10–70%) by the gas being sensed and a minimum of absorption by other constituents. This selection of intervals can readily be modified for future flights to improve performance or to sense other gases. We already anticipate moving the CO_2 sensing intervals to another spectral region. Since the CO_2 mixing ratio in the stratosphere is known, the data in these intervals were to be used for measuring atmospheric pressures (Park *et al.*, 1979). However, after the spectrometer was built, it was discovered that pressure-induced absorption by molecular nitrogen in the stratosphere, previously assumed to be negligible in these intervals, is probably not negligible (Rinsland *et al.*, 1981). Unfortunately, because this phenomenon lacks a firm theoretical foundation, calculations for long paths in the stratosphere are uncertain, and this uncertainty will propagate into the inferred atmospheric pressures; hence the decision to locate these intervals in another spectral region.

3. Observations

Supported by the balloon at an altitude of 39 km, the instrument collected data for several hours until sunset. Fig. 2 shows the observing geometry at an instant during the critical 30 min before sunset, the "occultation" period. During this period the solar zenith

Unauthenticated | Downloaded 05/19/25 12:36 PM UTC

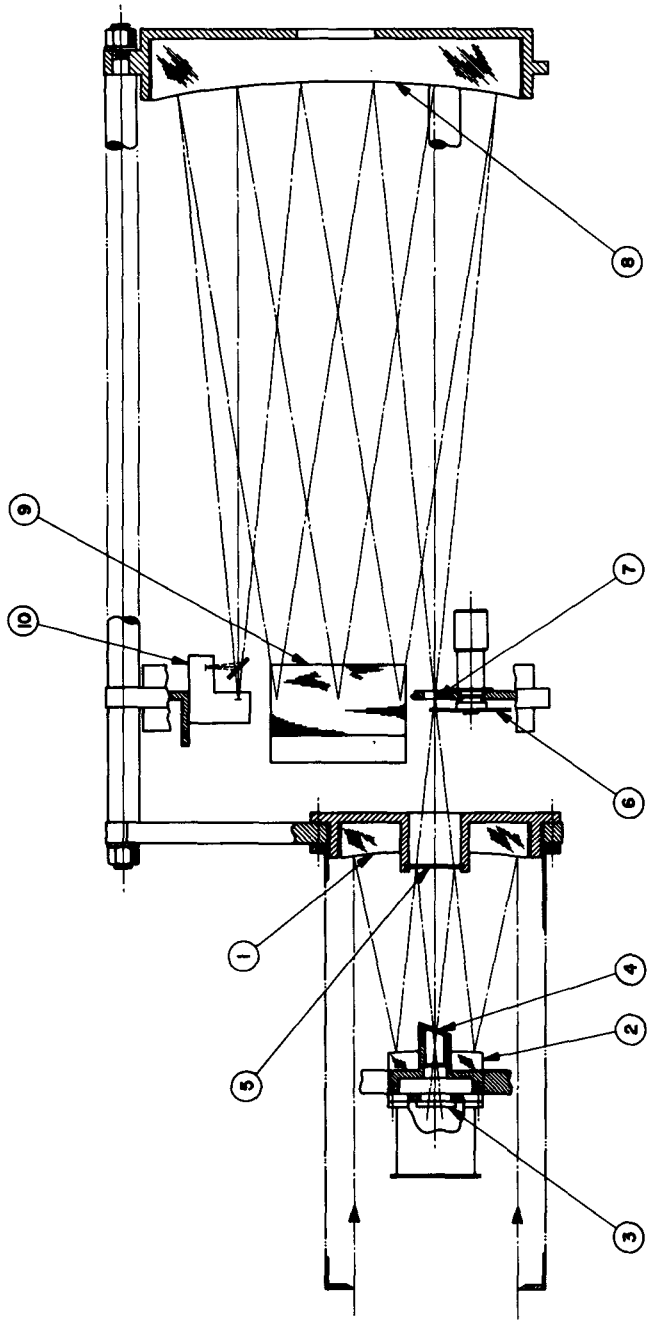

FIG. 1. Layout of instrument showing Cassegrain telescope with primary (1) and secondary (2) mirrors, sun-tracker (3) with its 2.18 μm narrow-band filter (4), and filter transmitting $\lambda > 3.5$ μm (5). The Ebert spectrometer contains a two-blade chopper (6), entrance slit (7), Ebert mirror (8), grating (9), and the detector array (10).

Unauthenticated | Downloaded 05/19/25 12:36 PM UTC

TABLE 1. Spectral intervals for balloon spectrometer.

Interval	Central wavenumber (cm^{-1})	Half-power bandwidth (cm^{-1})	Species
1	886	5	HNO_3
2	930	4	CF_2Cl_2
3	980	6	O_3 (low altitude)
4	998	6	O_3 (high altitude)
5	1507.0	3	H_2O (high altitude)
6	1528.5	4.5	H_2O (low altitude)
7	2385	4	CO_2 (high altitude)
8	2390	4	CO_2 (low altitude)

angles exceeded 90°, and the sun-to-balloon paths penetrated layers of the atmosphere below the balloon. Except for the fact that the balloon was not entirely outside the atmosphere, these observations simulated satellite observations. During this period, the tangent heights (the heights of the sun-to-balloon rays at their closest points to the earth) decreased from 39 to 12 km. Unfortunately, the solar tracker malfunctioned, and the instrument's field of view wandered away from the sun near the end of the period, limiting observations to the tangent heights between 39 and 25 km.

With the instrument at an altitude of 39 km, its angular field of view intercepted areas whose heights were ~1 km at the 25 km tangent point and 0.6 km at the 35 km tangent point. Throughout the experiment, the random noise in the data was very low. For the integration time of 1.5 s, the signal-to-noise was between 150/1 and 500/1, the higher values applying to the spectral intervals at the shorter wavelengths.

After the sun had set, the spectrometer slowly scanned upward in elevation, measuring emission from the region of the stratosphere that it had sounded just minutes before. The signals from the emission were hardly distinguishable from the instrument's electronic zero, and because they were so weak they appeared to be independent of elevation angle between −4° and +1°.

4. Conversion of raw data to transmittances

Although observations were confined to the upper stratosphere, there was enough absorption in intervals 1 and 3–6 for us to retrieve the concentrations of ozone, water vapor and nitric acid. However, the almost total transparency of the atmosphere in interval 2 prevented any retrievals of CF_2Cl_2. Also, for the reasons stated earlier, the measurements in intervals 7–8 were not used. Therefore, this paper concentrates on the retrievals of concentrations of water vapor, ozone and nitric acid.

The retrieval algorithms expect to receive measurements in the form of atmospheric transmission as a function of tangent height. In Figs. 3–5 the data are displayed in this form. They were obtained from the raw data by the following procedures: First, the time of observation was transformed to solar zenith angle by calculations based on the solar ephemeris. Then solar zenith angles were transformed to tangent heights via an atmospheric ray trace, which included effects of refraction.

To transform the solar signals from units of volts to transmittance, one has to divide them by the signals produced by the sun's radiation outside the atmosphere. In a satellite experiment at sunset, such unattenuated signals are directly measured before the occultation period. However, in this experiment the spectrometer was embedded in the atmosphere, and

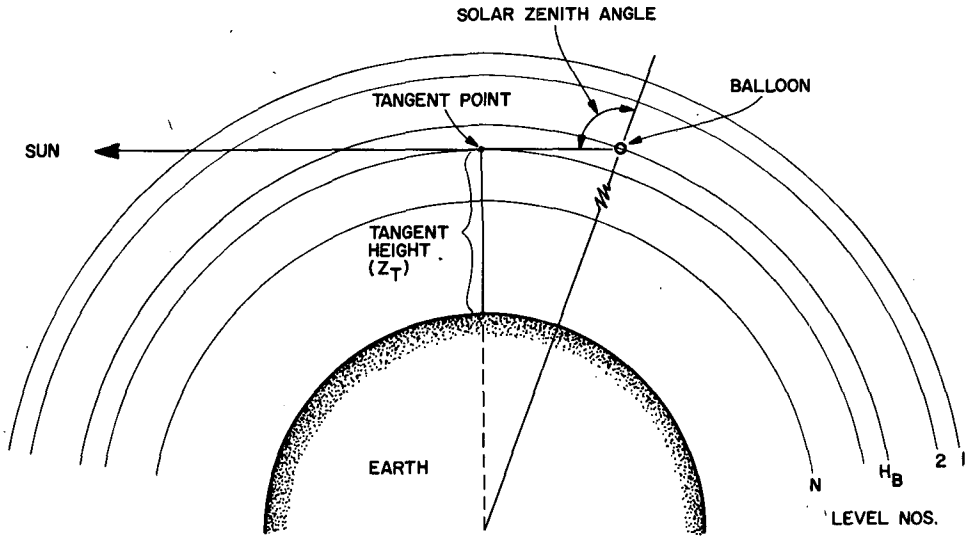

FIG. 2. Solar occultation geometry.

Unauthenticated | Downloaded 05/19/25 12:36 PM UTC

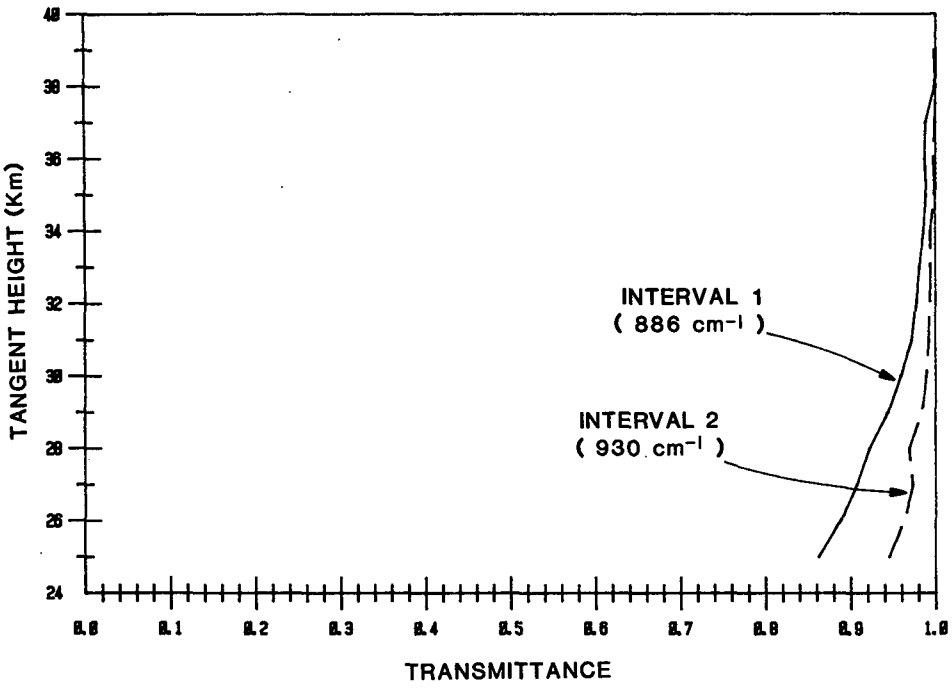

FIG. 3. Measured transmittances vs tangent height for nitric acid and Freon-12.

although only a fraction of a percent of the atmosphere lay above the balloon (atmospheric pressure at the balloon altitude was 3.6 mb), it still could slightly attenuate the radiation. In intervals 1 and 2, it was assumed that the atmosphere above the balloon was totally transparent. This assumption is corroborated both by the measurements themselves and by theoretical calculations. Therefore, in intervals 1 and 2, the unattenuated signals are the measurements made before the sun's zenith angle reached 90°.

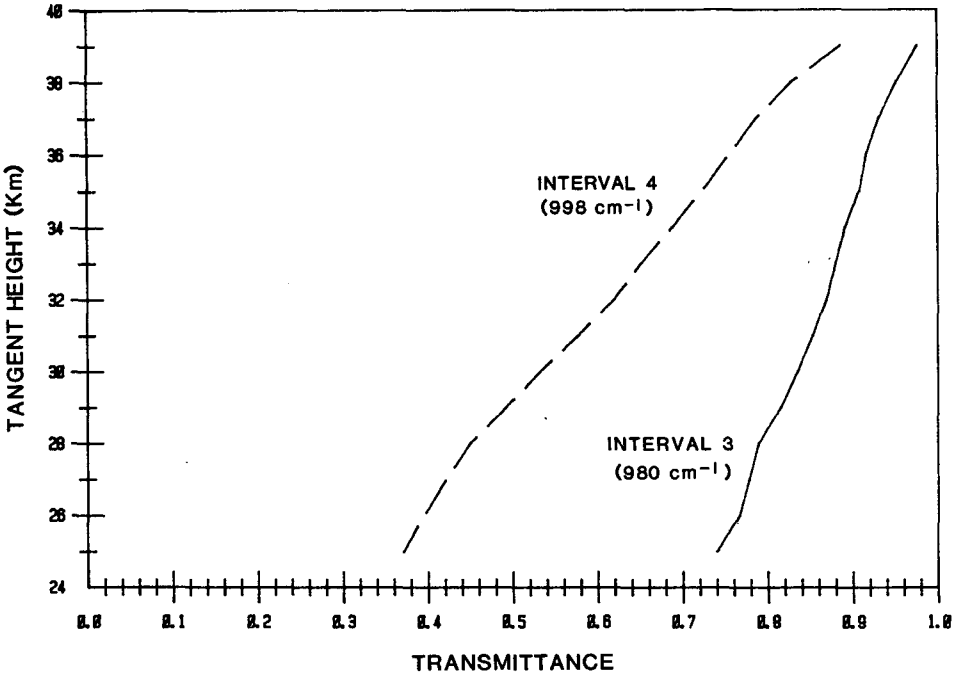

FIG. 4. As in Fig. 3, but for ozone transmittances.

Unauthenticated | Downloaded 05/19/25 12:36 PM UTC

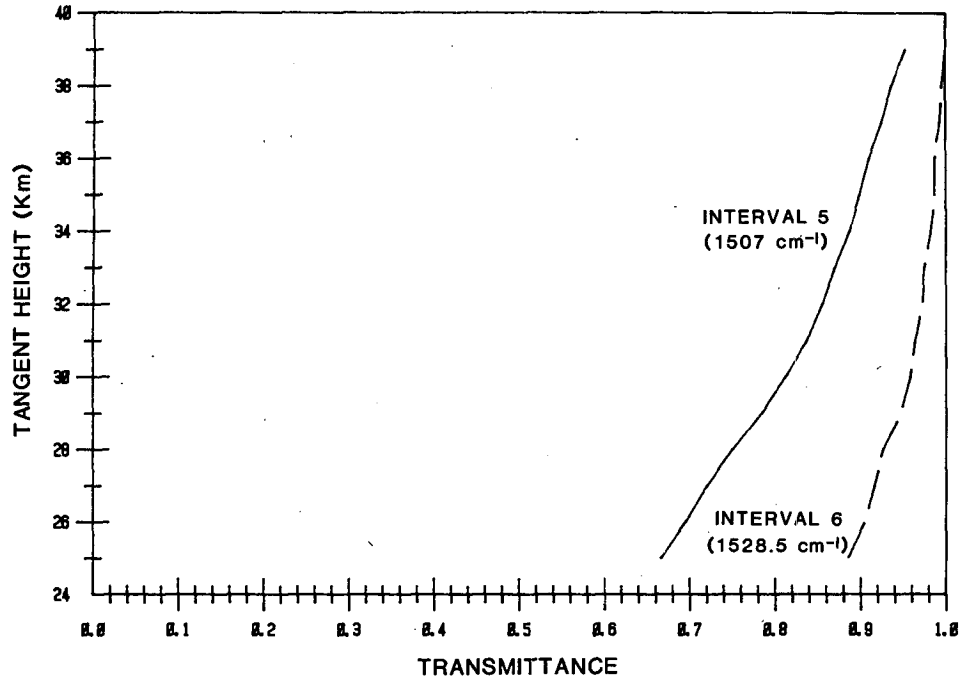

FIG. 5. As in Fig. 3, but for water vapor transmittances.

In intervals 3–6, the atmosphere above the balloon was not totally transparent. Even before the sun's zenith angle reached 90°, the radiation in these intervals had suffered some absorption. In consequence, the unattenuated signals were inferred from the relation,

$$N(i) = N(2)[G(i)/G(2)][S(i)/S(2)], \quad (1)$$

where N is the unattenuated signal (expressed in volts), i the interval number, G the gain of the instrument (output volts/input radiance), and S the solar radiance. The quantity $N(2)$, the unattenuated signal in interval 2, was measured during the flight, as described in the preceding paragraph. The values of G were measured in tests conducted in a vacuum chamber before the flight. The ratios of the solar radiance were taken from the literature (Thekaekara, 1971). Interval 2 was used as the basis for this procedure because it is the interval in which the upper atmosphere absorbs the least.

5. Computations

a. Transmittance calculations

1) GENERAL APPROACH

An important part of the data analysis is the computation of transmittances through the stratosphere between the sun and the balloon. These transmittances are averages over the spectrometer's spectral response functions, which are essentially triangles in plots of response vs wavenumber, with their centers and widths specified in Table 1. Although the line-by-line approach is the most accurate one for computing transmittances, it is too cumbersome to be used in routine data analysis. Instead we used methods that are more efficient, while being almost as accurate when they are averaged over the spectral intervals of the instrument and restricted to the limited ranges of pressures, temperatures and gas concentrations that stratospheric limb paths have. The general approach was first, before the balloon flight, to define analytic transmittance functions for homogeneous paths, i.e., paths having uniform pressures, temperatures and concentrations; then, in the analysis of the flight data, to apply these functions to produce transmittances through limb paths, as described below.

In all the numerical work, the atmosphere was treated as an onion-like composite of 1 km thick concentric spherical shells, each shell having a constant pressure, temperature and gas concentration (see Fig. 2). These variables are functions of altitude. The total absorber amount was computed from the integral of the concentration over the limb path, which included effects of atmospheric refraction.

2) OZONE

The analytic transmittance function is a variation on the Smith polynomial (Smith, 1969). For each of the two ozone intervals, the transmittance τ is given by

$$\ln(-\ln\tau) = \sum_{j=1}^{14} \alpha_j X_j, \quad (2)$$

Unauthenticated | Downloaded 05/19/25 12:36 PM UTC

where the independent variables X_j are given by

$$\left.\begin{aligned} X_1 &= 1, & X_2 &= 0.1\ln(UT/273), & X_3 &= \ln(P/1000) \\ X_4 &= \ln(T/273), & X_5 &= X_2X_3, & X_6 &= X_2X_4 \\ X_7 &= X_2^2, & X_8 &= X_4X_7, & X_9 &= X_3X_4 \\ X_{10} &= X_2X_7, & X_{11} &= X_3X_5, & X_{12} &= X_3^2 \\ X_{13} &= X_3X_6, & X_{14} &= X_3X_7 \end{aligned}\right\}$$

and where U is the ozone amount in units of 1.25×10^{19} molecules cm^{-2}, P the pressure (mb), and T the temperature (K).

We evaluated the coefficients α_j by fitting the polynomial to line-by-line calculations (Neuendorffer, 1977) for a set of 140 homogeneous paths. The combinations of P, T and U in these paths include the full range of values they take in the stratosphere. The line-by-line calculations used spectral line parameters from the 1980 version of the AFGL line parameters compilation (Rothman, 1981). The resulting α_j appear in Appendix A.

We applied the method of Weinreb and Neuendorffer (1973) to these polynomials to calculate transmittances through the limb paths. This is an iterative method that replaces the path between the sun and the nth level of the atmosphere by an homogeneous path whose "equivalent" absorber amount is computed from the absorption that occurred in the path between the sun and the $(n-1)$st level.

3) WATER VAPOR

The analytic transmittance function is again given by Eq. (2), where U is in units of grams per square centimeter. We evaluated the coefficients α_j as we did those for ozone, except that here a set of 50 homogeneous paths was used. The α_j again appear in Appendix A.

To apply these functions in computing transmittances in limb paths, we reduced each limb path to an equivalent homogeneous path by a simple two-parameter scaling approximation,

$$\left.\begin{aligned} T_e(U; Z_T) &= U^{-1}\int_0^U T(u)du \\ P_e(U; Z_T) &= U^{-1}\int_0^U P(u)du \end{aligned}\right\}, \qquad (3)$$

where the integrals are carried out over the limb paths, making them depend on the tangent heights Z_T. The values of T_e and P_e obtained in this way can be thought of as "mass-weighted" mean values for the limb path.

4) NITRIC ACID

Unlike ozone and water vapor, the transmittances for nitric acid are not based on line-by-line calculations, because the spectral line parameters are not yet compiled near 886 cm^{-1} for this gas. Instead, we applied the statistical band model as formulated by Goldman *et al.* (1981), i.e.,

$$\ln\tau = -k(T)U(1 + \beta U/P)^{-1/2}, \qquad (4)$$

where β and k are the wavenumber-dependent constants of the model, and U is the amount of nitric acid (atm-cm). Since $\beta U/P \ll 1$, it was set equal to zero. Values of k, corresponding to averages over 5 cm^{-1} intervals, are tabulated at four temperatures in Goldman *et al.* (1981). We fitted the temperature-dependence of the absorption coefficient by

$$k(T) = k(294)\left(\frac{294}{T}\right)^n, \qquad (5)$$

where for the spectral interval centered at 886 cm^{-1}, $k(294) = 13.3$ cm^{-1} atm^{-1}, and $n = 0.4$.

In applying Eqs. (4) and (5) to the atmosphere, we replaced T with a mass-weighted value [Eq. (3)].

b. *Inverse algorithm*

When measurements are made from a satellite, the mathematical problem is to derive concentrations at levels 1, 2, ..., N from transmittances measured through paths with tangent points numbered 1, 2, ..., N (see Fig. 2). However, from a balloon the measurements are made only for paths with tangent points numbered H_B, $H_B + 1$, ..., N, where H_B is the index of the level at the altitude of the balloon. In this experiment, $H_B = 8$ and $N = 22$. For nitric acid, which is sensed in only one spectral interval, this gives 15 measurements to determine concentrations at 22 levels. To avoid having more unknowns than equations, we fix the concentrations at the levels above the balloon at a reasonable initial estimate, and retrieve only at the levels below the balloon. In principle this will introduce errors in the solution, especially at the levels at and immediately below the balloon, but in this experiment this is a relatively unimportant source of error. The main error source is that there is practically no measurable absorption from the layers above and just below the balloon, so in any case the retrieval will not provide much information at these levels.

For the constituents sensed in two spectral intervals, i.e., ozone and water vapor, the number of measurements is 30. Hence for these gases we can at least

Unauthenticated | Downloaded 05/19/25 12:36 PM UTC

attempt to retrieve the concentrations at levels above the balloon. (Of course, the main objective is to retrieve at levels below the balloon.)

In either case, the system of equations to be solved is

$$\tau_k(C_1, \ldots, C_L) + \epsilon_k = t_k, \quad k = 1, 2, \ldots, K,$$

where K, the number of equations, is 15 for nitric acid and 30 for ozone and water vapor. The number of levels L at which concentrations are retrieved is 15 for nitric acid and 22 for water vapor and ozone. In this equation t represents measured transmittances, τ the calculated transmittances, C the unknown concentrations, and ϵ the unknown errors, whose sources are both measurement and calculation.

To avoid the instabilities encountered in inverting such a system of equations, we applied a simple iterative version of the Levenberg-Marquardt algorithm (see, for example, Lawson and Hanson, 1974). A description of this algorithm is presented in Appendix B.

c. *Sources of error*

We propagated the rms values of the random instrument-related errors through the retrieval algorithm to estimate the random errors in the retrieved profiles. In spectral intervals 1 and 2, the main error sources are random errors in the observations and the possibility of short-term drift in system gain. Together they contribute an rms error of under 1% of the measured transmittances. However, in the other spectral intervals, the uncertainties are larger, because to infer unattenuated solar signal levels in these intervals, we need to apply laboratory measurements, via Eq. (1), to account for the non-transparency of the atmosphere above the balloon, as described in Section 4. The resultant estimates of the rms random error in the measured transmittances are between 2.0 and 2.5% of the measured transmittances. To propagate rms transmittance errors through the retrieval algorithm, we performed the retrievals both before and after perturbing the measured transmittances by an error equal to the rms transmittance error whose effect we are interested in. The difference between the two retrieved profiles of concentrations was interpreted as the rms of the random errors in the retrievals.

Systematic errors also affect the accuracy of the retrieved profiles, but since their magnitudes are unknown, we could not estimate their effects. Three of the most likely sources of such errors deserve mention. First, it is possible that water vapor from the troposphere, carried aloft by the balloon and instrumentation, could have contaminated the optical path in or near our instrument. To guard against this, the launch was timed so that the instrument "baked" in the sun for hours before sunset. In addition, the instrument was constructed to be as open to the atmosphere as possible so that internal water vapor could escape as rapidly as possible. The main consequence of this error source would be that the retrieved water vapor concentrations would be too high. However, from the results shown in the following section, we can conclude that there was little problem from this source.

A second possible error source is that the instrument's field of view might be offset from the sun's center. This would cause the measured transmittances to be assigned to an incorrect tangent height, thereby introducing a retrieval error. This problem would be most severe at the lowest altitudes, where sun-tracking is most difficult, and where errors in pointing angle transform geometrically to the largest errors in tangent height. Nevertheless, even at the lowest altitude, data from the sun-tracker indicate that the maximum pointing error was less than 1 km in tangent height.

Probably the most likely source of systematic error is in the computations, specifically the transmittance computations. For example, spectral line parameters are currently being revised, and phenomena such as temperature dependences of line widths are not clearly understood. In the case of nitric acid, where we applied a simple band model that was formulated from laboratory measurements to long stratospheric paths, the probability of significant error is high. [For a careful study of the effect of transmittance errors in limb-viewing experiments, see Smith and Gordley (1983).]

Because the balloon flight took place several months after the powerful eruption of the Mexican volcano El Chichon, the question arose as to whether the ensuing volcanic cloud could have affected the observations. At the time of the flight (June 21, 1982), the cloud was most dense at altitudes near 25 km (e.g., Adriani, *et al.*, 1983). Assuming it was present at the location of this experiment, the cloud might have induced extra absorption in the infrared measurements near 25 km, and hence it would have been manifested in the retrieved profiles as a tendency toward unexpectedly high, but incorrect, concentrations at these altitudes. However, according to the results presented in the next section, the retrievals show no such tendency. The effects of the cloud, if present, were too small to be detected by this experiment. This conclusion seems consistent with observations in the literature (e.g., Barth *et al.*, 1983) that the main body of the El Chichon cloud was confined to latitudes south of 30°N in June 1982, whereas the area sounded in this experiment was north of 32°N.

6. Results

a. *Ozone*

Figure 6 shows the retrieval of the ozone concentrations (solid profile). The error bars represent the positive and negative estimated rms random instrument-related errors, as described in the previous section. (The full length of each bar is twice the rms

Unauthenticated | Downloaded 05/19/25 12:36 PM UTC

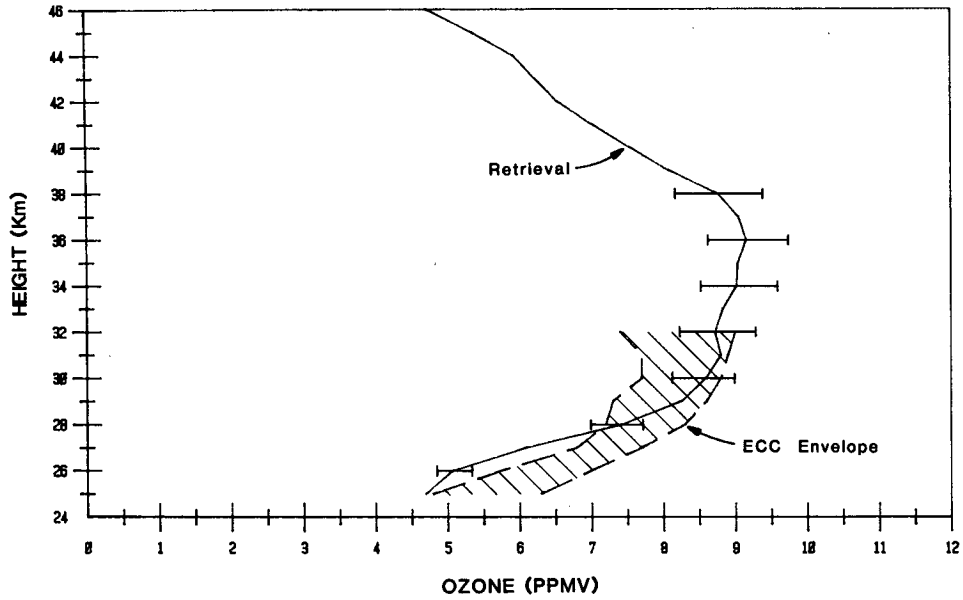

FIG. 6. Retrieved ozone mixing ratio as a function of tangent height, and ECC envelope.

error.) The retrievals are specified at levels spaced every kilometer in altitude, but the error bars are attached only to alternate points to keep the figure from being too crowded. Also shown in the figure is an envelope of six *in-situ* profiles measured by balloon-borne Electro-Chemical Concentration Cells (ECC's; Komhyr, 1969). These measurements were made at Palestine, which is several hundred kilometers southeast of the location of the retrieved profile, in the period beginning 48 hours before the flight of our instrument and ending 48 hours after. The profiles were normalized to total ozone determinations made with Dobson spectrophotometers at Palestine. At altitudes above 25 km, the six ECC soundings exhibited a considerable random variability, with peak-to-peak differences of the order of 1 ppmv, and because of this the figure shows only their envelope. Overall there is good agreement between the retrieval and the ECC data. Only at 26–27 km is the difference between them larger than the estimated uncertainties.

Because of the lack of ECC data above 32 km and its volatility below, we sought data from another source to demonstrate that the retrieval is at least typical of this location and season. Fig. 7 displays a comparison between the retrieval and a profile inferred from measurements made near Palestine in June 1979 by the Solar Back-scattered Ultra-Violet sensor on the Nimbus-7 satellite.[2] Since the two observations were made three years apart, the SBUV profile is not to be regarded as "ground truth," but the general similarity between the two profiles does indicate that the retrieval is indeed typical of soundings for the location and season.

Figure 8 illustrates the dependence of the retrieval on the first-guess profile, which is used to start the iterative retrieval process. "Guess 1" is a constant 5 ppmv, and "Guess 2" is the mid-latitude model of Krueger and Minzner (1976). (Guess 2 was the basis for the retrieval shown in Figs. 6 and 7.) Although the two guesses differ drastically at all altitudes, the retrievals differ significantly from each other only above 38 km. Below 28 km they are virtually identical. Hence, at most altitudes, the retrievals are nearly independent of their guesses, which is a desirable result. This behavior is consistent with the fact that for tangent heights below 38 km, there is a strong signal (i.e., absorption) from the atmosphere (see Fig. 4), which obviously "controls" the retrievals. On the other hand, the levels above 38 km give weak signals, permitting the retrievals at these levels to retain more of the characteristics of their initial guesses.

It is also significant that although neither guess resembles the ECC envelope (Fig. 6) or the SBUV profile (Fig. 7), the retrieval does. Thus, the information in the measurements seems to be influencing the retrievals toward a more realistic estimate of the actual conditions.

b. Water vapor

Figure 9 shows the water vapor retrieval. It is specified at 1 km intervals, while the error bars are attached every 2 km. From the error bars we see that the measurement uncertainty ranges from ±50% at 38 km to

[2] SBUV data available from National Space Science Data Center, National Aeronautics and Space Administration, Goddard Space Flight Center, Greenbelt, MD 20771.

Unauthenticated | Downloaded 05/19/25 12:36 PM UTC

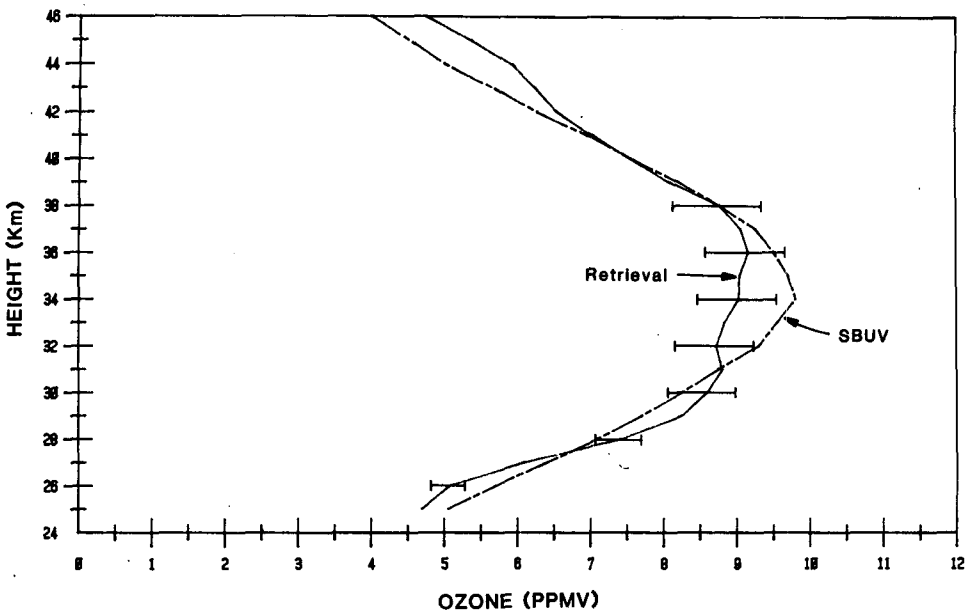

FIG. 7. Retrieved ozone mixing-ratio profile and SBUV data from 1979.

±10% at 26 km. The large uncertainties at the upper levels are a consequence of the low signal (i.e., high transmittance) from the atmosphere at these levels (see Fig. 5). These results indicate that the 1507 cm^{-1} interval should be moved to a more "opaque" spectral region to enhance the signal from the upper stratosphere.

The second of the three profiles on Fig. 9 is the first-guess profile, 5 ppmv throughout the stratosphere. Lacking any *in-situ* data for comparison with the retrieval, we instead show in Fig. 9 a third profile, which was inferred from measurements made in May 1979 near Palestine by the Limb Infrared Monitor of the Stratosphere (LIMS) on the Nimbus-7 satellite. This profile is not to be thought of as the "truth," but as a representative of typical conditions, and the retrieval resembles it. As further evidence of the reasonableness of the retrieval, the reader is referred to Figs. 5 and 6 in a recently published review on stratospheric water vapor (Ellsaesser, 1983). Those figures are a compi-

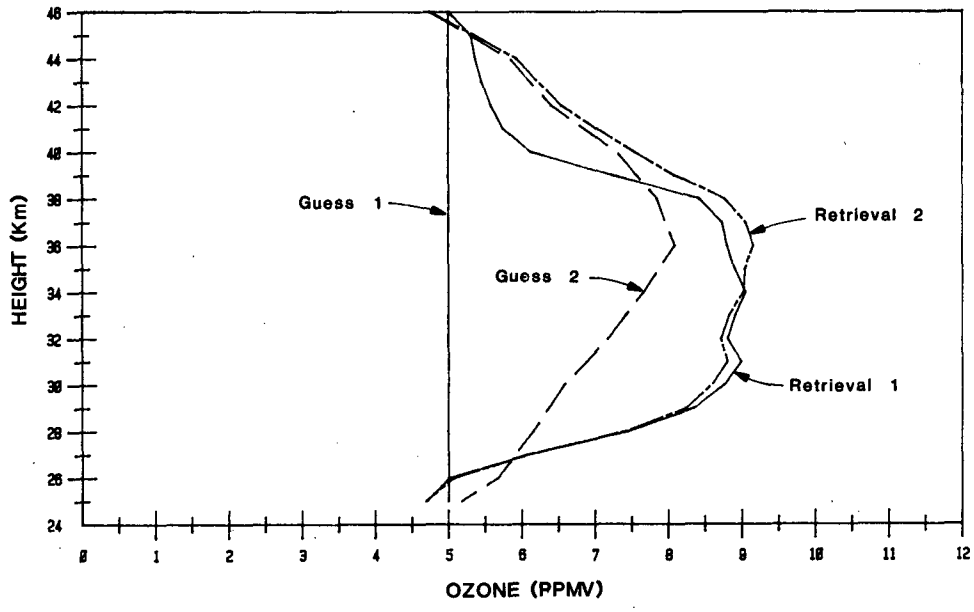

FIG. 8. Dependence of retrieved ozone mixing-ratio profile on first-guess profile.

Unauthenticated | Downloaded 05/19/25 12:36 PM UTC

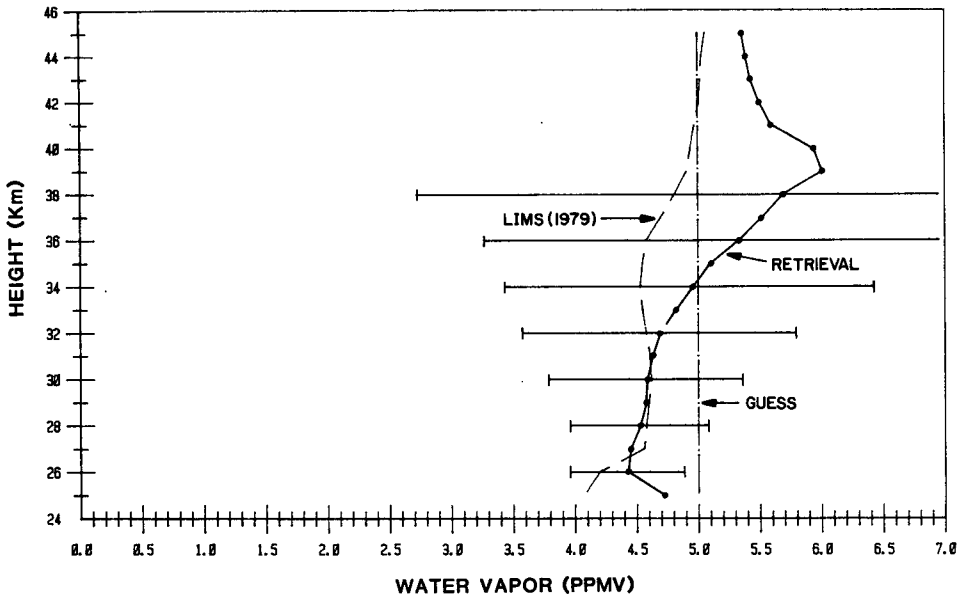

FIG. 9. Retrieved water vapor mixing-ratio profile, first-guess profile, and LIMS data from 1979.

lation of measurements of water vapor profiles. In the 25–39 km range, the retrieval is close to the mean of the measurements shown by Ellsaesser.

c. *Nitric acid*

Figure 10 shows the retrieval of the nitric-acid concentrations. The error bars, derived as described earlier, signify the measurement uncertainties. According to the data in Fig. 3, the atmospheric signal from nitric acid is weak, and this is reflected in the error bars, especially at the highest altitudes. Below 28 km, the uncertainties are relatively small, being of the order of ±10%. With such weak signals, how did this come about? The reason is that the instrument-related random noise is low in the nitric-acid-sensing channel, because as mentioned earlier, we could determine the unattenuated solar signal in this channel without recourse to laboratory measurements and Eq. (1).

The guess for the nitric acid retrieval is a polar-

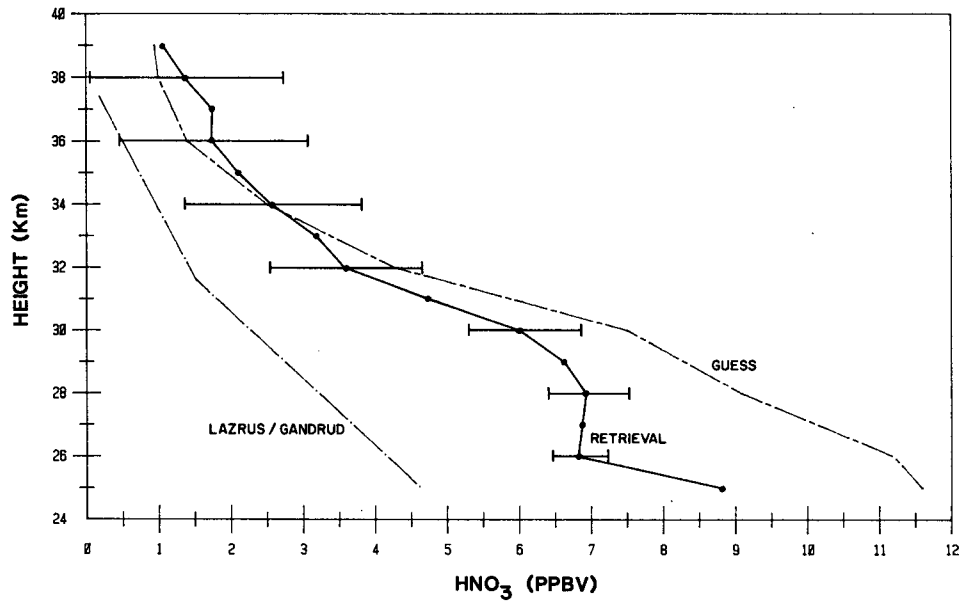

FIG. 10. Retrieved nitric acid mixing-ratio profile, first-guess profile, and 1973 *in-situ* data (Lazrus and Gandrud, 1974).

Unauthenticated | Downloaded 05/19/25 12:36 PM UTC

winter profile compiled by the LIMS Experiment Team. This profile approximates an upper bound for measurements of nitric acid. No *in-situ* measurements were available to be compared with the nitric acid retrieval. However, the retrieval is typical of the measurements presented in Fig. 4-12 of Hudson and Reed (1979). This reference also mentions that the measurements by the *in-situ* technique of sorption on cellulose filters (Lazrus and Gandrud, 1974) give significantly lower values of nitric-acid concentration than do those by remote techniques. The measurement of Lazrus and Gandrud (1974) that was made near Palestine in the spring of 1973 is included in Fig. 10 as a lower bound.

7. Conclusions and discussion

This experiment demonstrates that infrared solar occultation data, acquired continuously in discrete spectral intervals with a moderate-resolution, nonscanning spectrometer, can be interpreted to yield realistic profiles of the concentrations of ozone, water vapor and nitric acid in the stratosphere. The rms of the uncertainties in the inferred concentrations range approximately from 5 to 10% for ozone, 10 to 50% for water vapor, and 10 to 100% for nitric acid, the largest errors corresponding to measurements at the highest altitudes, where the atmosphere is most transparent. For water vapor and ozone, much of the uncertainty results from procedures for eliminating effects of the nontransparent atmosphere above the balloon. This error source will not exist in measurements from satellites. Moreover, in future experiments we hope to reduce the uncertainties in the water vapor measurements above 30 km by relocating one of the spectral intervals in a spectral region of stronger absorption.

Even with the moderately wide (~ 5 cm^{-1}) spectral intervals of this instrument, the atmosphere provides enough signal (i.e., absorption) for sensing ozone and water vapor confidently to altitudes of 39 km and probably higher. In the case of nitric acid, however, the signal strength, and hence the retrievable information, above 35 km is low and can be increased only with higher resolution, which will be attainable to some extent with a larger satellite version of the spectrometer.

These measurements are also subject to many of the systematic errors (e.g., errors in pointing and in transmittance calculations) that beset most remote measurements, but their effects could not be determined in the absence of complete, reliable *in-situ* measurements.

These results provide an encouraging start in testing this technique's feasibility for monitoring concentrations of many of the important stratospheric trace species from satellites. We plan more balloon flights to extend the soundings to lower altitudes, to measure the concentrations of other gases, and at the same time to obtain better *in-situ* data.

Acknowledgments. The authors are grateful for the extensive support contributed by Mr. Walter R. Nagel and his group from the Attitude Control and Stabilization Branch of the National Aeronautics and Space Administration, Goddard Space Flight Center. They provided the gondola, telemetry, arrangements for the balloon flight, and much useful advice. We appreciate the expert services of the National Scientific Balloon Facility at Palestine, Texas in launching and recovering the balloon package. We thank Drs. David G. Murcray and Aaron Goldman of the University of Denver for allowing us access to unpublished atmospheric spectra and for valuable advice. Credit for optical design belongs to Mr. Donald F. Hansen and his staff at HSS, Inc., Bedford, MA. Mr. Michael L. Hill of NOAA/NESDIS is to be acknowledged for his invaluable programming services. The ECC ozone measurements were provided by Mr. Harry Bloxom and his group at the National Aeronautics and Space Administration, Wallops Flight Center. The SBUV ozone profile was supplied by Mr. A. J. Miller of NOAA/NMC/Climate Analysis Center and the LIMS water vapor and nitric acid profiles by Mr. Walter G. Planet of NOAA/NESDIS.

APPENDIX A

TABLE A1. Polynomial coefficients (α_j) for transmittance calculations.

j	980 cm^{-1}	998 cm^{-1}	1507 cm^{-1}	1528.5 cm^{-1}
1	−3.5192	−0.5452	3.1785	3.4323
2	10.5016	8.1181	2.2172	7.4284
3	−0.2455	0.2319	0.1832	0.7061
4	6.7642	2.5919	−0.1274	−0.7787
5	−0.2966	−0.3772	−0.8599	0.5384
6	−3.7748	0	0.2378	−1.8916
7	−1.7020	−4.3236	−2.5662	1.3354
8	0.5589	−0.1509	−0.2806	−0.9054
9	0.4944	0.1576	0.7524×10^{-1}	−0.1258
10	0	1.9631	−0.2034	-0.5240×10^{-1}
11	−0.1325	−0.1305	-0.4707×10^{-1}	0
12	-0.3716×10^{-1}	-0.6080×10^{-2}	-0.2881×10^{-1}	1.9422×10^{-3}
13	0.5074×10^{-3}	2.2300	0.1420	−0.1797
14	0.8472	0	−0.4811	0.3793

APPENDIX B

Inverse Algorithm

The system of equations to be solved is

$$\tau_k(C_1, \ldots, C_L) + \epsilon_k = t_k, \quad k = 1, 2, \ldots, K,$$

where $K \geqslant L$. In this equation t represents the measured transmittances, τ the calculated transmittances, C the unknown concentrations, and ϵ the unknown errors, whose sources are both measurement and calculation. To invert this system of equations, we apply a simple version of the Levenberg-Marquardt algorithm (see, e.g., Lawson and Hanson, 1974). Denote the column

Unauthenticated | Downloaded 05/19/25 12:36 PM UTC

vector of concentrations $C_1, \ldots, C_L$ by $\mathbf{C}$, and the vectors of computed and measured transmittances by τ and $\mathbf{t}$, respectively. It should be noted that τ is a nonlinear function of $\mathbf{C}$. Therefore, we perform the inversion iteratively, beginning with an initial estimate $\mathbf{C}^{(0)}$, and then generating a sequence of approximate solutions, $\mathbf{C}^{(1)}, \mathbf{C}^{(2)}, \ldots, \mathbf{C}^{(i)}, \mathbf{C}^{(i+1)}, \ldots$. In the $(i+1)$st step, we attempt to minimize the length of $\tau(\mathbf{C}) - \mathbf{t}$ while simultaneously minimizing the departure of the solution $\mathbf{C}^{(i+1)}$ from $\mathbf{C}^{(i)}$. Specifically, we minimize the quadratic form

$$Q = \|\tau(\mathbf{C}) - \mathbf{t}\|^2 + \lambda^2\|\mathbf{C} - \mathbf{C}^{(i)}\|^2,$$

where λ is a smoothing parameter. Since τ is a nonlinear function of $\mathbf{C}$, we linearize it locally by a Taylor expansion,

$$\tau(\mathbf{C}) \approx \tau(\mathbf{C}^{(i)}) + \mathbf{J}^{(i)}(\mathbf{C} - \mathbf{C}^{(i)}),$$

in which the matrix $\mathbf{J}^{(i)}$ is the Jacobian matrix $\{\partial\tau_k/\partial C_l\}$ evaluated at $\mathbf{C}^{(i)}$. Combining the two preceding equations, we obtain

$$Q^{(i)} = \|\tau(\mathbf{C}^{(i)}) + \mathbf{J}^{(i)}(\mathbf{C} - \mathbf{C}^{(i)}) - \mathbf{t}\|^2 + \lambda^2\|\mathbf{C} - \mathbf{C}^{(i)}\|^2, \quad \text{(B1)}$$

which is the quadratic form to be minimized in each iteration. Minimizing $Q^{(i)}$ is equivalent to solving the linear least-squares problem,

$$\begin{bmatrix}\mathbf{J}^{(i)} \\ \lambda\mathbf{I}_L\end{bmatrix}(\mathbf{C} - \mathbf{C}^{(i)}) \approx \begin{bmatrix}\mathbf{t} - \tau(\mathbf{C}^{(i)}) \\ \mathbf{0}_L\end{bmatrix},$$

where $\mathbf{I}_L$ is the $L \times L$ identity matrix, and $\mathbf{0}_L$ is a column of L zeroes. The solution is derived in Lawson and Hanson (1974, pp. 190–192). Briefly, we begin with a singular-value decomposition of $\mathbf{J}^{(i)}$: [For simplicity, we will suppress many of the superscripts (i), the iteration number.]

$$\mathbf{J} = \mathbf{USV}^{\mathrm{T}},$$

where $\mathbf{J}$ is a $K \times L$ matrix, $\mathbf{U}$ an orthogonal $K \times K$ matrix, $\mathbf{V}$ an orthogonal $L \times L$ matrix, and $\mathbf{S}$ a $K \times L$ matrix of the form

$$\begin{bmatrix}\sigma_1 & & & \\ & \sigma_2 & & \mathbf{0} \\ & & \ddots & \\ & & & \sigma_L \\ \mathbf{0} & & & \end{bmatrix}.$$

The singular values σ_l are in order of decreasing magnitude, i.e.,

$$\sigma_1 \geq \sigma_2 \geq \cdots \sigma_L \geq 0.$$

Let n be the number of non-zero singular values ($n \leq L$). We now define the vector

$$(a_1, \ldots, a_K)^{\mathrm{T}} \equiv U^{\mathrm{T}}[\mathbf{t} - \tau(\mathbf{C}^{(i)})].$$

Next, we define the vector $\mathbf{y}$, whose elements are given by

$$y_l = \begin{cases} a_l\sigma_l/(\sigma_l^2 + \lambda^2), & \text{for } 1 \leq l \leq n \\ 0, & \text{for } l > n. \end{cases} \quad \text{(B2)}$$

Then the solution is given by

$$\mathbf{C}^{(i+1)} = \mathbf{C}^{(i)} + \mathbf{Vy}.$$

The Levenberg-Marquardt method is a convenient method for generating a sequence of concentration profiles that minimize $\|\tau - \mathbf{t}\|$. By having the term $\lambda^2\|\mathbf{C} - \mathbf{C}^{(i)}\|^2$ in Eq. (B1), we are able to restrict the size of $\|\mathbf{C}^{(i+1)} - \mathbf{C}^{(i)}\|$ so that the Taylor expansion of $\tau(\mathbf{C})$ is sufficiently accurate. The minimization of Q [Eq. (B1)] will therefore more likely lead to the minimization of $\|\tau - \mathbf{t}\|$. Without such a constraint on $\|\mathbf{C}^{(i+1)} - \mathbf{C}^{(i)}\|$ it is well known that $\mathbf{C}^{(i+1)}$ often can move away from $\mathbf{C}^{(i)}$ to give an unduly large value of $\|\tau - \mathbf{t}\|$. The singular value decomposition also provides a convenient rule for choosing λ to assure that $\|\mathbf{C}^{(i+1)} - \mathbf{C}^{(i)}\|$ is not excessively large—this is especially likely when $\mathbf{J}^{(i)}$ has a condition number σ_1/σ_n significantly larger than the machine precision. Using Eq. (B2) as a guide, we choose λ so that it is smaller than the largest singular value σ_1 but within one or two orders of magnitude of σ_1.

The algorithm is applied iteratively until $\|\tau(\mathbf{C}) - \mathbf{t}\|/K^{-1/2}$ becomes less than a preset value, typically 0.01, which is approximately the instrument noise. For the ozone and nitric acid retrievals, the number of iterations was two; for water vapor it was six.

REFERENCES

Adriani, A., F. Congeduti, G. Fiocco and G. P. Gobbi, 1983: One-year lidar observations of the stratospheric aerosol at Frascati, March 1982–March 1983. *Geophys. Res. Lett.*, **10,** 1005–1008.

Barth, C. A., R. W. Sanders, R. J. Thomas, G. E. Thomas, B. M. Jakosky and R. A. West, 1983: Formation of the El Chichon aerosol cloud. *Geophys. Res. Lett.*, **10,** 993–996.

Ellsaesser, H. W., 1983: Stratospheric water vapor. *J. Geophys. Res.*, **88,** 3897–3906.

Farmer, C. B., O. F. Raper, B. D. Robbins, R. A. Toth and C. Muller, 1980: Simultaneous spectroscopic measurements of stratospheric species: O_3, CH_4, CO, CO_2, N_2O, H_2O, HCl, and HF at northern and southern mid-latitudes. *J. Geophys. Res.*, **85,** 1621–1632.

Girard, A., J. Besson, L. Gramont and E. Haziza, 1977: Spectrometre automatique aeroporte pour la surveillance des gaz a l'etat de trace dans la haute atmosphere. *Météorologie,* **10,** 3–14.

Goldman, A., F. S. Bonomo, F. P. J. Valero, D. Goorvitch and R. W. Boese, 1981: Temperature dependence of HNO_3 absorption in the 11.3 μm region. *Appl. Opt.*, **20,** 172–175.

——, R. D. Blatherwick, F. J. Murcray, J. W. Van Allen, F. H. Murcray and D. G. Murcray, 1982: Atlas of stratospheric IR absorption spectra. *Appl. Opt.*, **21,** 1163–1164.

Hudson, R. D., and E. I. Reed, 1979: The stratosphere: present and future. *NASA Reference Publication 1049,* NASA Goddard Space Flight Center, Greenbelt, Md., 432 pp.

Komhyr, W. D., 1969: Electrochemical concentration cells for gas analysis. *Ann. Géophys.*, **25,** 203–210.

Krueger, A. J., and R. A. Minzner, 1976: A mid-latitude ozone

Unauthenticated | Downloaded 05/19/25 12:36 PM UTC

model for the 1976 U.S. Standard Atmosphere. *J. Geophys. Res.*, **81,** 4477–4481.

Lawson, C. L., and R. J. Hanson, 1974. *Solving Least Squares Problems.* Prentice-Hall, 189–192.

Lazrus, A. L., and B. W. Gandrud, 1974: Distribution of stratospheric nitric acid vapor. *J. Atmos. Sci.*, **31,** 1102–1108.

Murcray, D. G., F. H. Murcray and W. J. Williams, 1967: A balloon-borne grating spectrometer. *Appl. Opt.*, **6,** 191–196.

——, A. Goldman, F. H. Murcray, F. J. Murcray and W. J. Williams, 1979: Stratospheric distribution of ClO NO_2. *Geophys. Res. Lett.*, **6,** 857–859.

Neuendorffer, A. C., 1977: Rapid atmospheric transmittance through fast Fourier convolution. *J. Opt. Soc. Amer.*, **67,** 1376.

Park, J. H., J. M. Russell III and S. R. Drayson, 1979: Pressure sensing of the atmosphere by solar occultation using broadband CO_2 absorption. *Appl. Opt.*, **18,** 1950–1954.

Rinsland, C. P., M. A. H. Smith, J. M. Russell III, J. H. Park and C. B. Farmer, 1981: Stratospheric measurements of continuous absorption near 2400 cm^{-1}. *Appl. Opt.*, **20,** 4167–4171.

Rothman, L. S., 1981: AFGL atmospheric absorption line parameters compilation: 1980 version. *Appl. Opt.*, **20,** 791–795.

Smith, M. A. H., and L. L. Gordley, 1983: Sensitivity of ozone retrievals in limb-viewing experiments to errors in line-width parameters. *J. Quant. Spectros. Radiat. Transfer,* **29,** 413–418.

Smith, W. L., 1969: A polynomial representation of carbon dioxide and water vapor transmission, ESSA Tech. Rep. NESC 47, National Environmental Satellite Center, 20 pp.

Thekaekara, M. P., 1971 (Second Printing—1973): Solar electromagnetic radiation. *NASA Space Vehicle Design Criteria Monograph,* NASA SP-8005, Goddard Space Flight Center, Greenbelt, MD, 37 pp.

Weinreb, M. P., and A. C. Neuendorffer, 1973: Method to apply homogeneous-path transmittance models to inhomogeneous atmospheres. *J. Atmos. Sci.*, **30,** 662–666.

Unauthenticated | Downloaded 05/19/25 12:36 PM UTC